Babalou, Milad; Torkaman, Hossein; Pouresmaeil, Edris; Pourmoradi, Nazanin

Fault Tolerant Dual Active Bridge Converter for Electric Vehicle Application

Published in:
Iranian Journal of Electrical and Electronic Engineering

DOI:
10.22068/IJEEE.20.2.2916

Published: 01/06/2024

Document Version
Publisher's PDF, also known as Version of record

IUST
Iran University of Science and Technology

Iranian Journal of Electrical and Electronic Engineering

Journal Homepage: ijeee.iust.ac.ir

Research Paper

Fault Tolerant Dual Active Bridge Converter for Electric Vehicle Application

Milad Babalou*, Hossein Torkaman*(C.A.), Edris Pouresmaeil**, Nazanin Pourmoradi*

Abstract: In this paper, a dual-active bridge converter based on the utilization of two transformers is presented. The principles of operation, switching strategy, and transmission power characteristics of the proposed converter under normal operation are discussed, comprehensively. Moreover, the RMS current of two transformers with different values of inductances of the inductors that are in series with the transformers; is discussed. The operation of the proposed dual active bridge (DAB) converter under the open-circuit failure of transformers is studied. In addition, the loss distribution of the proposed converter in different powers is investigated. The proposed dual-transformer-based dual-active bridge converter is compared with the presented converters. Finally, the proposed converter with a low-voltage side (VL= 300 V), the switching frequency of power MOSFETs (fs= 50 kHz), and an accurate model of the electric battery at a high-voltage side (VH= 450 V) are simulated to verify the way of charging and discharging the electrical battery with the proposed converter under normal and open-circuit fault of transformers.

Keywords: Dual Active Bridge Converter, Dual-Transform-Based, Open-Circuit, Fault-Tolerant, Electric Vehicles.

1 Introduction

POWER electronics are crucial devices in power transmission [1-8]. Among various types of converters, bidirectional DC-DC converters are widely used in energy storage systems such as battery electric vehicles (BEVs), as shown in Fig. 1. Particularly, the dual active bridge converter (DAB) is an ideal choice for this application [9-14]. Simple and symmetrical structure, soft switching of power switches with zero-voltage switching (ZVS), incorporating a high-frequency transformer for isolation, high power density, and the ability of bidirectional power transmission are benefits of the DAB that make it an excellent candidate for use in energy storage systems for BEVs [15, 16].

Recently, researchers have introduced various switching strategies for DAB converters such as single-phase-shift (SPS), dual-phase-shift (DPS), and triple-phase-shift (TPS) [17]. Additionally, different types of DAB converter structures have been suggested, divided into two categories- current source and voltage source. Some examples of voltage source converters are the full-bridge and half-bridge conventional dual active bridge converters. A DAB current source converter for high-current and low-voltage applications is presented in [18]. In this presented converter, the input current is continuous due to using an inductor on the input side, and soft switching under zero current (ZCS) is possible. Dual active bridge converters can be categorized into two types, two-level and multi-level, based on the input and output voltage level of the transformer. To reduce the voltage stress of semiconductors, the multi-level structure of dual-active bridge converters is utilized [19]. Other types of DAB converters have also been proposed, which feature resonant tank LC, LLC, CLLC structures, etc. [20]. The soft switching property of these converters increases their frequency functional area, which leads to increased power density.

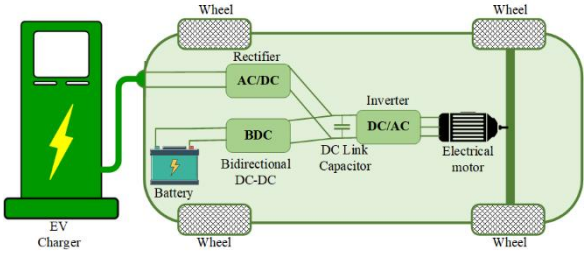

Fig .1 Application of BDC converter in electric vehicles.

Iranian Journal of Electrical & Electronic Engineering, 2024.
Paper first received 29 May 2023 and accepted 04 May 2024.
* The authors are with the Faculty of Electrical Engineering, Shahid Beheshti University, Tehran, Iran.
E-mail: m_babalou@sbu.ac.ir., h_torkaman@sbu.ac.ir, nazaninpourmoradi77@gmail.com ,
** The author is with the Department of Electrical Engineering and Automation, Aalto University, Espoo, Finland.
E-mails: edris.pouresmaeil@aalto.fi
Corresponding Author: Hossein Torkaman.

DAB converters can be categorized according to the number of transformers they employ, namely: single-transformer, dual-transformer, or multi-transformer DAB converters. Dual-transformer-based DAB converters are designed to reduce power stress on high-frequency transformers and offer better power density by utilizing a smaller transformer core compared to their single-transformer counterparts. Recent studies have introduced improved dual-transformer-based DAB converters. In [21], the unified segmental control strategies has been utilized in dual-transformer-based DAB converters to reduce conduction and switching losses. [22] presents a dual-transformer current-fed dual active bridge technique that has been developed to optimize the peak of the leakage inductor current and alleviate the current stress experienced by power switches, thereby enhancing the converter's overall efficiency. However, this particular DAB converter is constrained in terms of increased power density due to the implementation of two DC inductors on the input side. On the other hand, [23] proposes a DAB converter using two transformers that exhibits a high zero voltage switching range, resulting in reduced power stress on the transformers. Similarly, [24] and [25] discuss DAB converters that utilize two transformers, leading to a reduction in power stress on these components.

All reviewed papers based on two transformers could not operate in open-circuit failure of a transformer. In this paper, a new DAB structure is introduced in which the proposed converter can continue to operate under the mentioned fault. In Section. 2, the proposed dual-transformer-based DAB under normal operation is studied, comprehensively. The proposed topology is discussed when the mentioned fault occurs in Section. 3. The efficiency of the converter is analyzed in Section. 4. The proposed converter is compared with other presented topologies in Section. 5. Finally, the proposed DAB is simulated in PLECS/PLEXIM software to validate the performance of topology in Section. 6.

2 The proposed DAB Topology

2.1 Description of Topology

The DAB converter proposed uses a dual-transformer structure, which is shown in Fig. 2. It has 6 power switches (S_{p1}, S_{p2}; S_{p3}, S_{p4}, S_{p5}, and S_{p6}) and 4 power switches (S_{s1}, S_{s2}, S_{s3}, and S_{s4}) on the low and high-voltage sides, respectively. The converter also includes two high-frequency transformers T_{r1} and T_{r2}, with the ratio of turns N_1 and N_2. Inductors L_1 and L_2 represent the total leakage inductance of the transformer and an additional inductor. On the high-voltage side, the converter has two electrolytic capacitors C_{H1} and C_{H2}, while on the low-voltage side, it only has one electrolytic capacitor (C_L).

2.2 Detailed Modes of the Proposed DAB Under Normal Performance

Fig. 3 illustrates the method for switching power MOSFETs and voltage and current waveforms of inductors L_1 and L_2. The MOSFETs S_{p6}, S_{s2}, and S_{s3} are turned on at a phase shift φ relative to S_{p1} and S_{p4}, while it is important to note that MOSFETs in the same leg should not be turned on together. Fig. 3 also displays the current waveforms of inductors, providing eight working modes for the converter. These modes' corresponding equivalent circuits are respectively shown in Fig. 4(a) to (h) and will be further discussed.

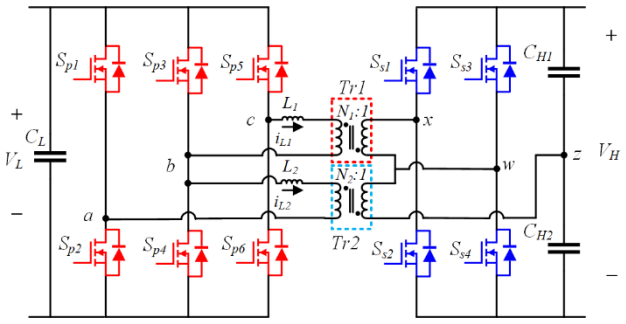

Fig. 2 The proposed dual-transformer-based DAB.

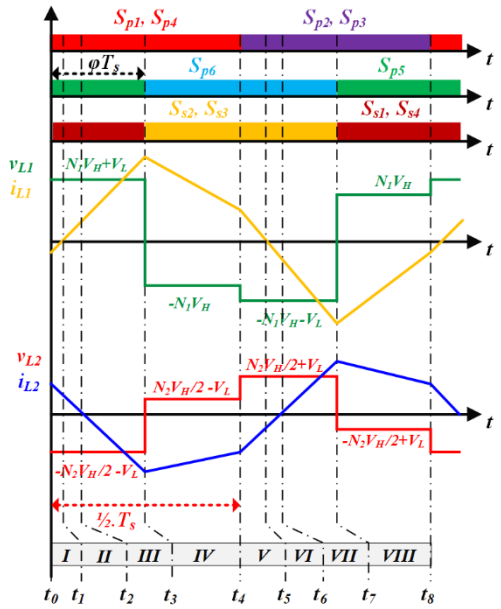

Fig. 3 Power MOSFETs switching strategy and current and voltage of inductors waveforms of the proposed DAB converter.

[t_0, t_1]: In the first stage shown in Fig. 4(a), the power switches S_{p1} and S_{p4} are instructed to turn on, and the anti-parallel diodes of MOSFETs S_{p1}, S_{p4}, S_{p5}, S_{s1}, and S_{s4} are activated. This stage ends when i_{L1} reaches zero.

$$i_{L1}(t) = \left[N_1 \cdot V_H + V_L \Big/ L_1 \right](t - t_0) + i_{L1}(t_0) \quad (1)$$

$$i_{L2}(t) = -\left[(N_2 \cdot V_H / 2) + V_L \Big/ L_2 \right](t - t_0) + i_{L2}(t_0) \quad (2)$$

[t_1, t_2]: The MOSFETs S_{p5}, S_{s1}, and S_{s4} are turned on under ZVS, and this stage concludes when i_{L2} reaches zero [cf. Fig. 4(b)].

[t_2, t_3]: When the current in the inductor L_2 drops to zero, the power switches S_{p1} and S_{p4} start conducting with ZVS. This stage continues until the S_{p5}, S_{s1}, and S_{s4} switches are turned off [cf. Fig. 4(c)].

[t_3, t_4]: At the start of this timeframe, S_{p6}'s anti-parallel diode on the primary side and S_{s2} and S_{s3} on the secondary side are conducted. S_{p1} and S_{p4} are also still operating [cf. Fig. 4(d)].

$$i_{L1}(t) = -\left[N_1 \cdot V_H \Big/ L_1 \right](t - t_3) + i_{L1}(t_3) \quad (3)$$

$$i_{L2}(t) = \left[(N_2 \cdot V_H / 2) - V_L \Big/ L_2 \right](t - t_3) + i_{L2}(t_3) \quad (4)$$

[t_4, t_5]: When the switches S_{p1} and S_{p4} are deactivated, it causes the anti-parallel diode of MOSFETs S_{p2} and S_{p3} to

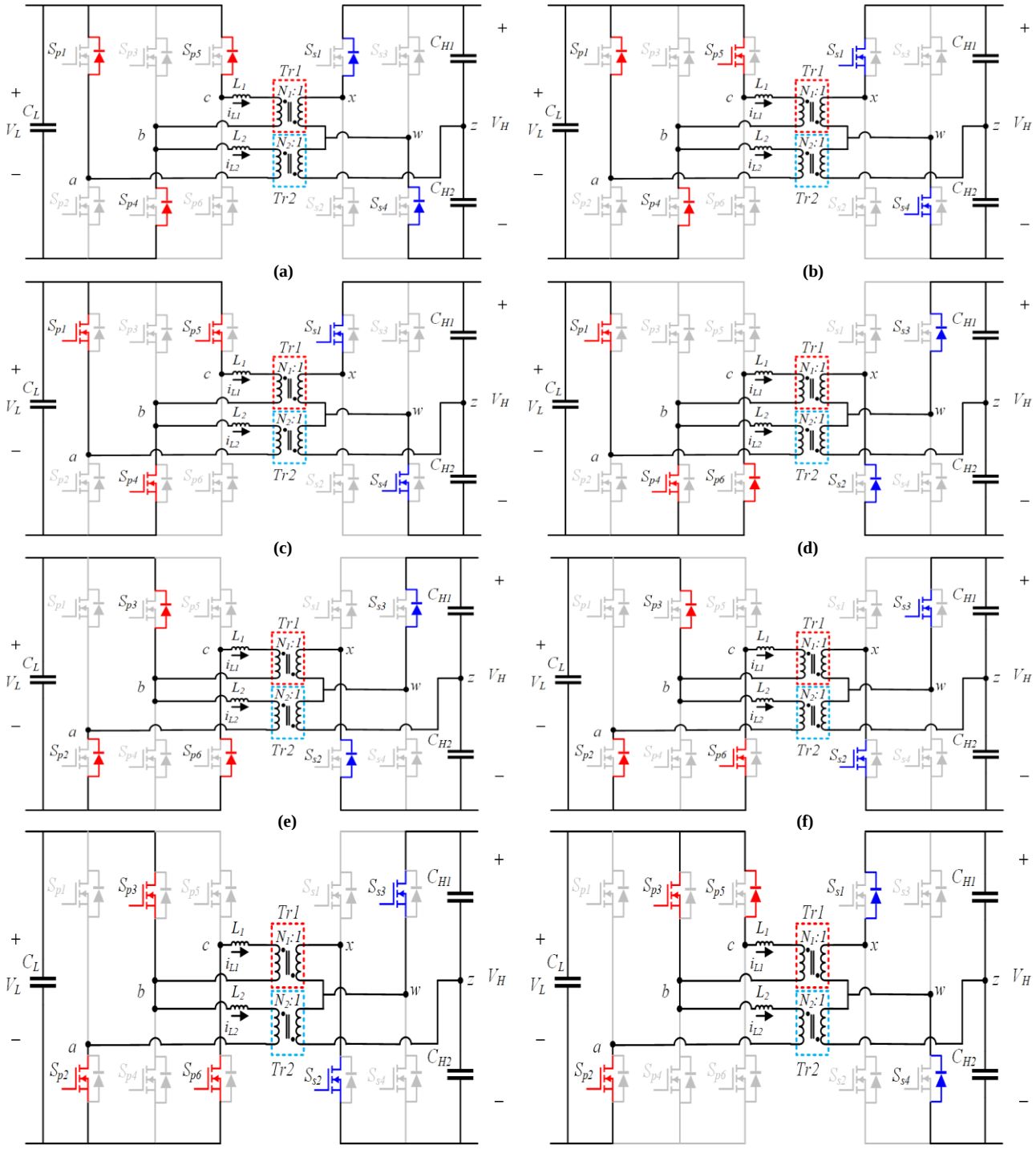

Fig. 4 Operation principles of the proposed DAB converter under normal operation; **(a)** [t_0, t_1]; **(b)** [t_1, t_2]; **(c)** [t_2, t_3]; **(d)** [t_3, t_4]; **(e)** [t_4, t_5]; **(f)** [t_5, t_6]; **(g)** [t_6, t_7]; **(h)** [t_7, t_8].

conduct. This state continues until the current flowing through i_{L1} reduces to zero [cf. Fig. 4(e)].

$$i_{L1}(t) = -\left[\frac{N_1 \cdot V_H + V_L}{L_1}\right](t - t_4) + i_{L1}(t_4) \quad (5)$$

$$i_{L2}(t) = +\left[\frac{(N_2 \cdot V_H / 2) + V_L}{L_2}\right](t - t_4) + i_{L2}(t_4) \quad (6)$$

[t_5, t_6]: S_{p6}, S_{s2}, and S_{s3} power switches operate with ZVS. As a result of this interval, the current flowing through i_{L2} reaches zero [cf. Fig. 4(f)].

[t_6, t_7]: Under the condition of ZVS, S_{p2}, and S_{p3} power switches are turned on. The end of this period is marked by the deactivation of the gate pulses associated with the MOSFETs S_{p6}, S_{s2}, and S_{s3} [cf. Fig. 4(g)].

[t_7, t_8]: The initiation of this interval, in which the anti-parallel diodes of S_{p5}, S_{s1}, and S_{s4} are conducted, is achieved by transmitting turn-on pulses to their respective gates [cf. Fig. 4(h)].

$$i_{L1}(t) = +\left[\frac{N_1 \cdot V_H}{L_1}\right](t - t_7) + i_{L1}(t_7) \quad (7)$$

$$i_{L2}(t) = -\left[\frac{(N_2 \cdot V_H / 2) - V_L}{L_2}\right](t - t_7) + i_{L2}(t_7) \quad (8)$$

2.3 Analysis of the Proposed DAB Power Under Normal Performance

In this section, the transmission power of the converter

transformers is discussed. To determine the initial current value of the inductors in a steady state, it should be set $i_{L1}(t_0)$ equal to $i_{L1}(t_8)$ for L_1 and $i_{L2}(t_0)$ equal to $i_{L2}(t_8)$ for L_2.

$$i_{L1}(t_0) = \frac{\left(\frac{1}{f_s} - 0.5\right)\left[|\varphi| V_L + \left(2|\varphi| - 0.5\right) N_1 V_H\right]}{L_1 f_s} \quad (9)$$

$$i_{L2}(t_0) = -\frac{\left(\frac{1}{f_s} - 0.5\right)\left[V_L + \left(2|\varphi| - 0.5\right) N_2 V_H\right]}{2 L_2 f_s} \quad (10)$$

The power transmission of transformer T_{r1} is derived from:

$$P_{Tr1} = \int_0^{T_s} v_{cb}(\tau)\, i_{L1}(\tau)\, d\tau \quad (11)$$

Consequently, P_{Tr1} will be as follows:

$$P_{Tr1} = \frac{\left[\varphi\left(0.5 - |\varphi|\right) N_1 V_H V_L\right]}{L_1 f_s} \quad (12)$$

Additionally, the power of the T_{r2} transformer's transmission can be derived from (13), which can also be expressed as (14):

$$P_{Tr2} = \int_0^{T_s} v_{ba}(\tau)\, i_{L2}(\tau)\, d\tau \quad (13)$$

$$P_{Tr2} = \frac{\left[\varphi\left(0.5 - |\varphi|\right) N_2 V_H V_L\right]}{L_2 f_s} \quad (14)$$

The overall transmission power would be the sum of the transmission powers of these two transformers:

$$P_{Total\_DAB} = P_{Tr1} + P_{Tr2} \quad (15)$$

By (12) and (14), it can be inferred that when the condition $N_1/L_1 = N_2/L_2 = N/L$ is met, P_{Total_DAB} is deduced as follows:

$$P_{Ttotal\_DAB} = \frac{\left[2\varphi\left(0.5 - |\varphi|\right) N V_H V_L\right]}{L f_s} \quad (16)$$

2.4 The Proposed DAB Power Sensitivity Under Normal Operation

This section covers the factors that affect the power of the proposed converter. Fig. 5(a) reveals that the transmitted power of transformers T_{r1} and T_{r2} is inversely proportional to the inductance. To demonstrate this correlation, we reduced the inductors from 200 µH to 100 µH (L_1=L_2), increasing transmitted power. Moreover, Fig. 5(b) shows a direct relationship between the transmitted power and the transformer's turn ratio which increase from 1.5 to 2 (N_1=N_2). The switching frequency of the converter is another determining factor that affects the transmitted power, as indicated by equation (16) and illustrated in Fig. 5(c). In other words, the output power of the proposed DAB is enhanced when the switching frequency of power MOSFETs is decreased from 75 kHz to 25 kHz. Additionally, the transmitted power is directly linked to the voltages of the low and high-voltage sides, as demonstrated in Fig. 5(d).

The basic power of the proposed DAB converter is as follows:

$$P_{Base} = \frac{N V_H V_L}{8 L f_s} \quad (17)$$

To normalize the output power of the dual transformer-based DAB converter under normal operating conditions, (16) is divided by (17) and the power characteristic shown in Fig. 6 is obtained.

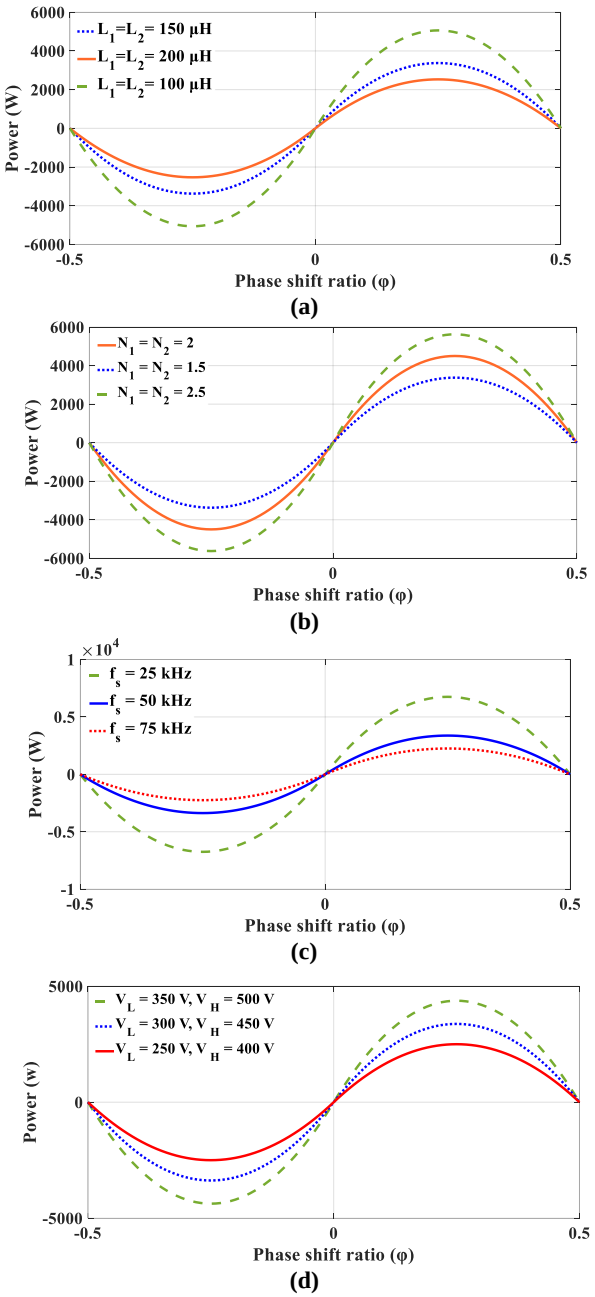

Fig. 5 Power curve characteristics of the proposed DAB with the variation of the; **(a)** inductors; **(b)** frequency; **(c)** turns ratio; **(d)** voltages.

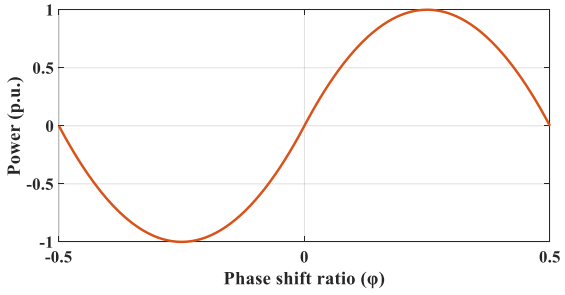

Fig. 6 Power curve of the proposed dual-transformer-based DAB in terms of p.u.

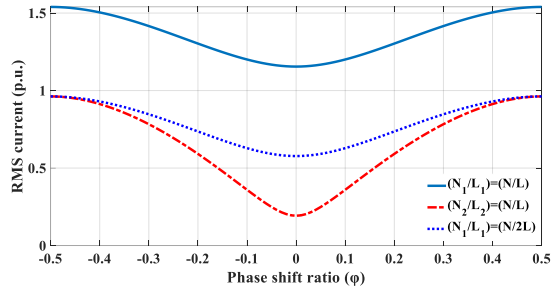

Fig. 7 The RMS current curve of the proposed DAB's transformers.

Table 1. Coefficients related to the RMS current

RMS current	Coefficients	Equation
$I_{L1,rms}$	a_1	$\left(192\varphi^2-96\varphi+12\right)T_s^{\,2}+1$
	a_2	$\left(192\varphi^2-48\varphi\right)T_s^{\,2}+\left(-32\varphi+24\right)\varphi^2$
	a_3	$\left(48\,T_s^{\,2}-16\,\varphi+12\right)\varphi^2$
$I_{L2,rms}$	b_1	$\left(192\varphi^2-96\varphi+12\right)T_s^{\,2}+1$
	b_2	$(192\varphi-48)T_s^{\,2}+\left(-128\varphi+96\right)\varphi^2-4$
	b_3	$48\,T_s^{\,2}+4$

2.5 Analysis of the RMS Current of DAB's Transformers

This section discusses the RMS current, a crucial factor in designing transformers. Table 1 provides coefficients for obtaining the RMS current at each transformer using equations (18) and (19). Fig. 7 displays results related to the RMS current of each transformer in p.u.. If the ratio of turns to inductance of one transformer is equal to the ratio of turns to the inductance of another transformer, the maximum RMS current passing through transformer Tr1 will be 54% higher than the base current. If the ratio is halved, the maximum RMS current passing through both transformers will be equal.

$$I_{L1,rms}=\left[\frac{a_1\left(N_1V_H\right)^2+a_2V_LN_1V_H+a_3V_L^{\,2}}{48\cdot\left(L_1\,f_s\right)^2}\right]^{1/2} \tag{18}$$

$$I_{L2,rms}=\left[\frac{b_1\left(N_2V_H\right)^2+b_2\,V_LN_2V_H+b_3V_L^{\,2}}{192\cdot\left(L_2\,f_s\right)^2}\right]^{1/2} \tag{19}$$

$$I_{Base}=\frac{N\,V_H}{8L\,f_s} \tag{20}$$

3 Detailed Performance of the Proposed DAB under Open-Circuit Failure of Transformer

3.1 Open-Circuit of Transformer T_{r1}

If the transformer T_{r1} experiences an open circuit fault, the proposed converter will operate according to the equivalent circuit shown in Fig. 8. It is worth mentioning

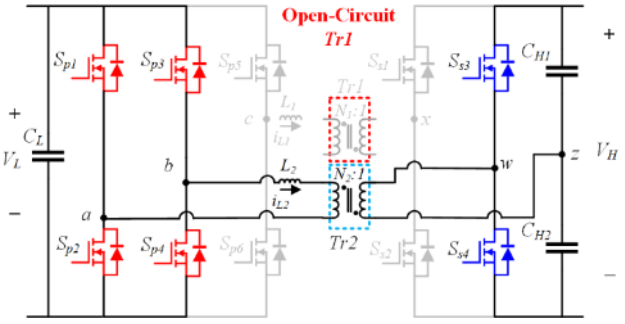

Fig. 8 The equivalent circuit of the proposed topology in the occurrence of open-circuit failure in T_{r1}.

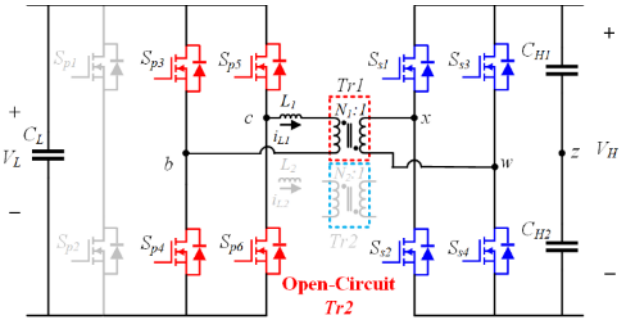

Fig. 9 The equivalent circuit of the proposed topology in the occurrence of open-circuit failure in T_{r2}.

that the converter can still function during this fault. However, the power MOSFETs S_{p5}, S_{p6}, S_{s1}, and S_{s2} will remain in the off state in this scenario. The converter's switching strategy remains the same as its normal operating mode, illustrated in Fig. 3. The voltage and current waveform of inductor L_2 will be similar to the normal operating mode, but the inductor current of L_1 will be zeroed out in case of this fault. The power passing through transformer T_{r1} will be zero, which results in the converter's output power being equivalent to the power passing through transformer T_{r2}.

$$P_{DAB\_OC,Tr1}=P_{Tr2} \tag{21}$$

3.2 Open-Circuit of Transformer T_{r2}

The corresponding equivalent circuit for the proposed converter in open-circuit failure of T_{r2} is illustrated in Fig.9. As a result of this issue, power MOSFETs S_{p1} and S_{p2} will always be turned off. Nonetheless, the converter's switching strategy is similar to its usual mode. The voltage and current waveform of inductor L_1 in this situation remain the same as those of the normal operating mode, except that the L_2 inductor current will be zeroed. Because no power flows through transformer T_{r2} when it is affected by an open circuit fault, the converter's power output will equal the power flowing through transformer T_{r1}.

$$P_{DAB\_OC,Tr2}=P_{Tr1} \tag{22}$$

4 Efficiency analysis of the proposed DAB

In this section, the losses of the proposed converter with specifications V_H=450 V, V_L= 300 V, f_s=50 kHz, N_1=N_2= 2, L_1=L_2=100 µH, ON resistance of MOSFETs (r_{DSON}= 23 mΩ), turn-on time of MOSFETs (t_{on}= 100 ns), turn-off time of MOSFETs (t_{off}= 169 ns), winding resistance of transformers on the low voltage side (r_{LL}= 2.2 mΩ), winding resistance of transformers on the high voltage side (r_{LH}= 4.4 mΩ), inductors resistance (r_{LI}= 1.2 mΩ),

and equivalent series resistance of capacitors (r_C= 10 mΩ) are calculated [26]. The distribution losses of the proposed converter in various powers are depicted in Fig. 10. The maximum power of the proposed converter is achieved with φ= 0.25 which is 6.4 kW. The efficiency is calculated at 91.58% as shown in Fig. 10 (a). The major and minor losses is related to conduction losses of power MOSFETs and inductor losses, respectively. There are two operating points for the proposed converter in the direct power transmission mode for a given specific power. For instance, there are two operating points of 0.15 and 0.34 for the power of 5.7 kW. Moreover, φ should be equal to 0.08 and 0.41 for the converter's performance at the power of 3.65 kW. According to Fig. 10 (b)-(e), it can be seen that when φ is between 0.25 and 0.5, the conduction losses of power MOSFETs will be higher. This is due to the circulating current in the transformers. Therefore, it is optimal for the converter to operate in the φ region between 0 and 0.25.

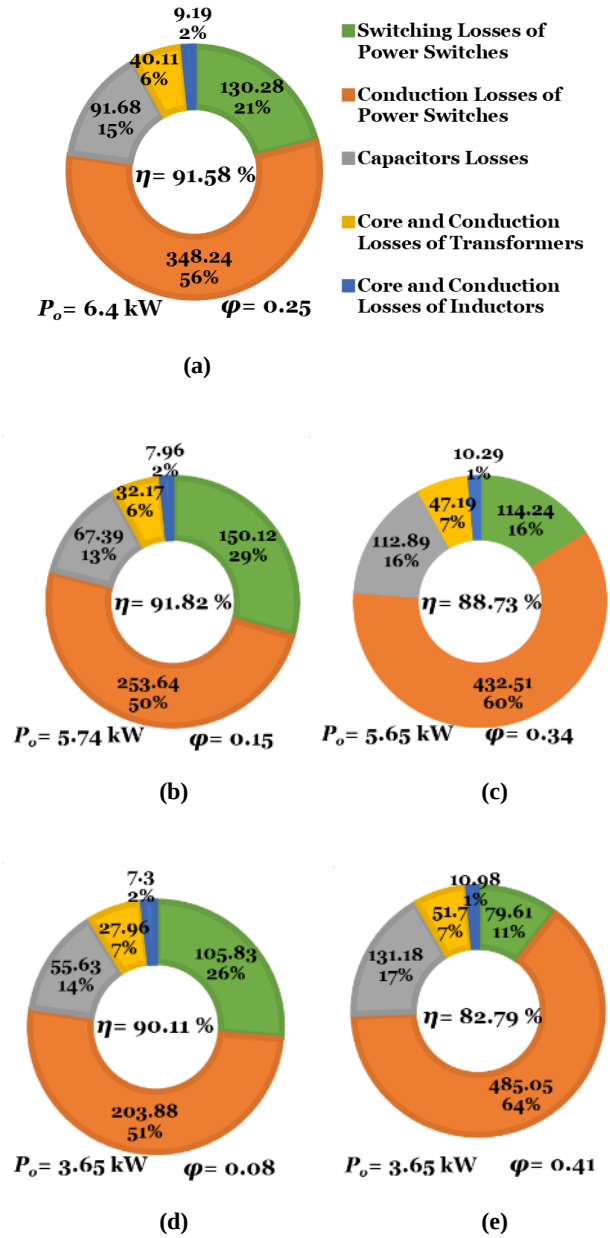

Fig. 10 Loss distribution of the proposed DAB converter under different output power and phase shift ratio; **(a)** 6.4 kW and φ=0.25; **(b)** 5.74 kW and φ=0.15; **(c)** 5.65 kW and φ=0.34; **(d)** 3.65 kW and φ=0.08; **(e)** 3.65 kW and φ=0.41.

Table. 2 Comparison of the proposed DAB converter with other referred topologies.

Ref.	Number of				P_{Output} (p.u.)	The capacity to perform even if one of the transformers experiences an open-circuit failure
	S^*	C^*	I^*	T^*		
[22]	6	4	1	2	0.28	✗
[23]	10	2	1	2	1	✗
[25]	10	3	1	2	0.89	✗
Prop.	10	3	2	2	1	✓
* *S*: Switches; *C*: Capacitors; *I*: Inductors, *T*: Transformers.						

5 Comparison of the Proposed DAB with other DAB topologies

In this section, the proposed converter is compared with the other dual-transformer-based DAB converters regarding the number of elements and the output power in terms of units, as given in Table. 2. The main benefit of the proposed converter, as mentioned in the previous sections, is the ability of the converter to continue operating even if an open-circuit fault occurs in one of the transformers. In case of this fault, considering the equal power passing through the power transformers, the rated power will be reduced by half. Also, the output power of the proposed converter is higher than the converters presented in [22] and [25].

6 Simulation Results

Table. 3 outlines the specifications for the proposed DAB converter, while PLEXIM/PLECS software is utilized to simulate the proposed dual-transformer-based DAB. The precise battery model presented in [27], with its corresponding specifications in Table. 4, is also employed on the high-voltage side. Additionally, an equivalent circuit of the battery simulated in PLECS is depicted in Fig. 11. The proposed converter is simulated in two modes: battery charging and battery discharging. In Fig. 12, the operation normal of the proposed DAB converter in charging mode (φ = 0.15) is illustrated. Moreover, the soft switching conditions of power MOSFETs is considered. In this operating point, the power MOSFETs S_{p3} and S_{p4} lost their ZVS turn-on conditions, as shown in Fig. 12 (f). The voltage stress of power switches in low and high-voltage sides are 300 V and 450 V, respectively.

Table. 3 The simulation specification of the proposed DAB converter

Capacitors (C_L= C_H)	460 µF
Inductors (L_1=L_2)	100 µH
Transformers (N_1=N_2)	2
Switching frequency	50 kHz
Maximum output power	6.4 kW
Low Voltage	300 V

Table. 4 The simulation specification of the battery on the high-voltage side

Number of series connected cells	117
Number of parallel branches	30
Target constant charging voltage for each cell	4.1 V
Target constant charging current for each cell	1.3 A
Initial SOC	50 %

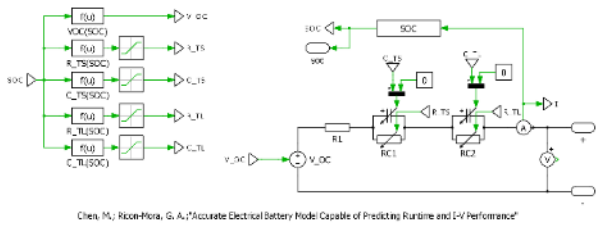

Fig. 11 The accurate battery model schematic in PLECS.

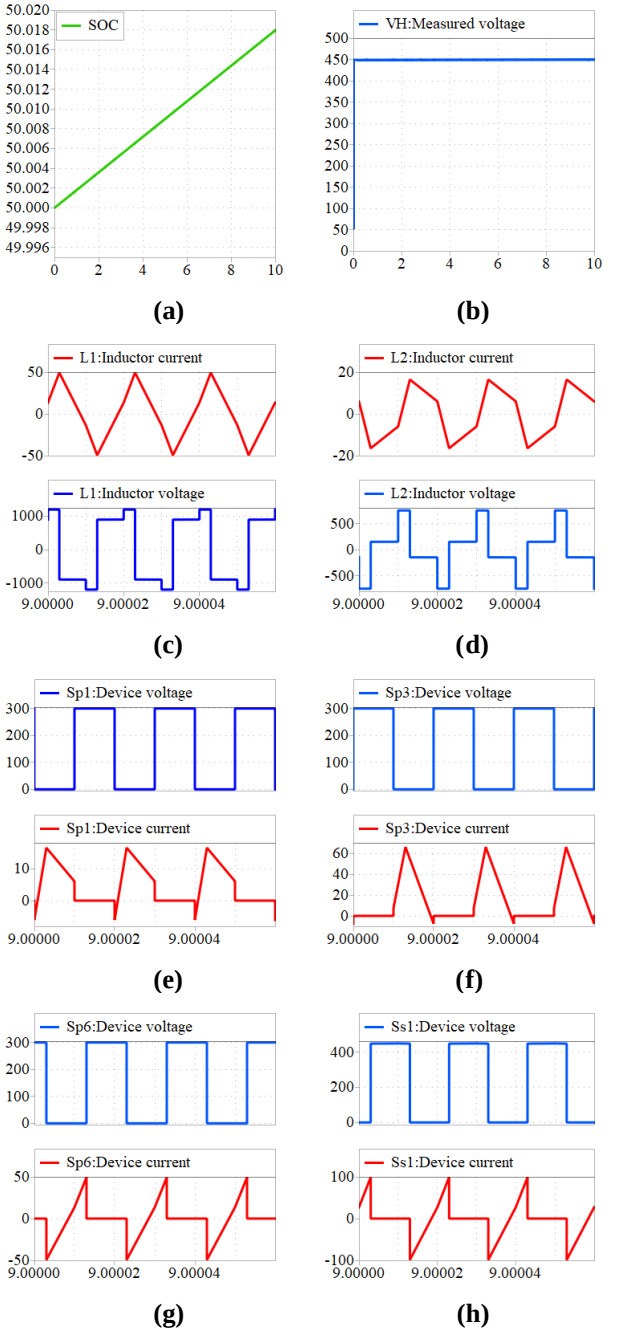

Fig. 12 The simulated outputs of the converter under normal operation in charging mode with φ = 0.15; **(a)** state of charge battery; **(b)** battery voltage; current and voltage of inductor **(c)** L_1; **(d)** L_2; voltage and current stress of power MOSFET **(e)** S_{p1}; **(f)** S_{p3}; **(g)** S_{p6}; **(h)** S_{s1}.

The simulation results of the proposed converter in charging mode with φ = 0.34 is depicted in Fig. 13. It is noteworthy that whole power switches are turned-on under ZVS. However, the current stresses of power MOSFETs are increased which affects the overall efficiency of the proposed DAB converter. For discharging mode, the proposed dual-transformer-based converter is simulated with φ = - 0.12 and the results are given in Fig. 14. As shown in Fig. 14 (a), the state of charge battery is reduced that validate the proposed converter can operate bidirectionally. Moreover, the power switches S_{p3} and S_{p4} are turned-on under hard switching conditions, as depicted in Fig. 14 (f). As mentioned previously, the proposed topology can operate under open-circuit failure of transformers. Hence, the simulation results in open-circuit faults of transformer T_{r1} and T_{r2} for charging mode with φ = 0.15 are illustrated in Fig. 15 and 16, respectively. As depicted in Fig. 15 (c), no power flow from transformer T_{r1} in the occurrence of fault in transformer T_{r1}. Moreover, the current stress of S_{p5}, S_{p6}, S_{s1} and S_{s2} is zero, as shown in Fig. 15 (g) and (h). It should be noted that the voltage stresses of power MOSFETs in this situation are the same as normal operation. When the fault occurs in transformer T_{r2}, the inductor current L_2 is zero, as illustrated in Fig. 16(d). In addition, the S_{p1} and S_{p2} is not conducted as Fig. 16 (e).

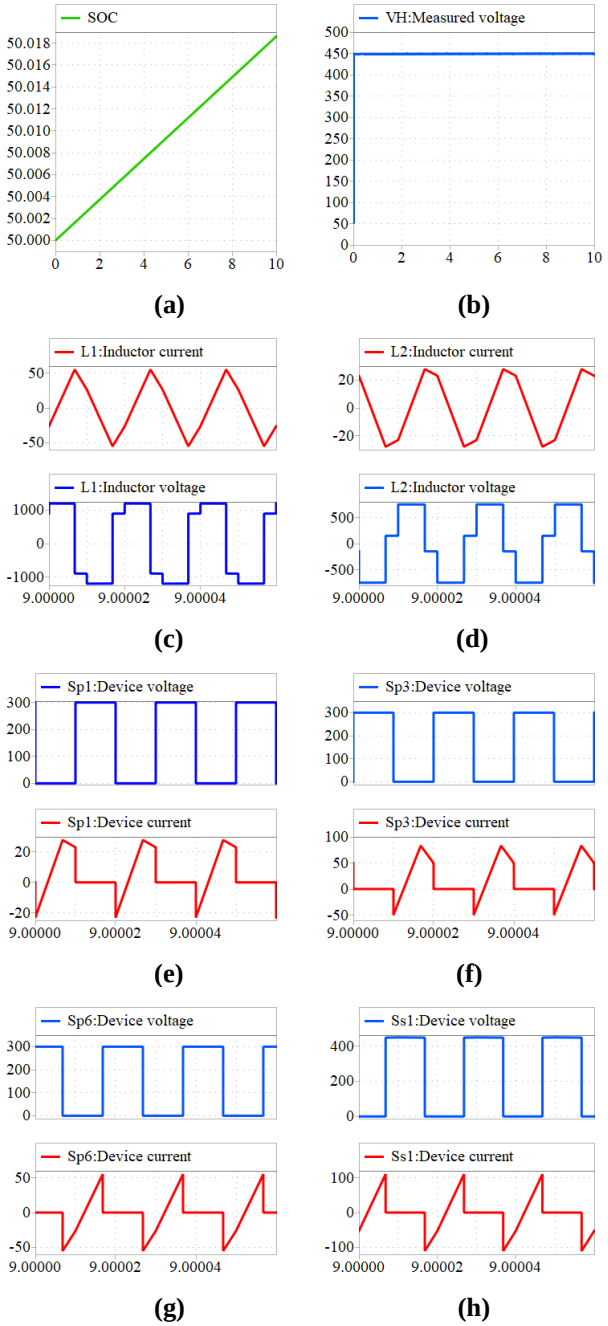

Fig. 13 The simulated outputs of the converter under normal operation in charging mode with φ = 0.34; **(a)** state of charge battery; **(b)** battery voltage; current and voltage of inductor **(c)** L_1; **(d)** L_2; voltage and current stress of power MOSFET **(e)** S_{p1}; **(f)** S_{p3}; **(g)** S_{p6}; **(h)** S_{s1}.

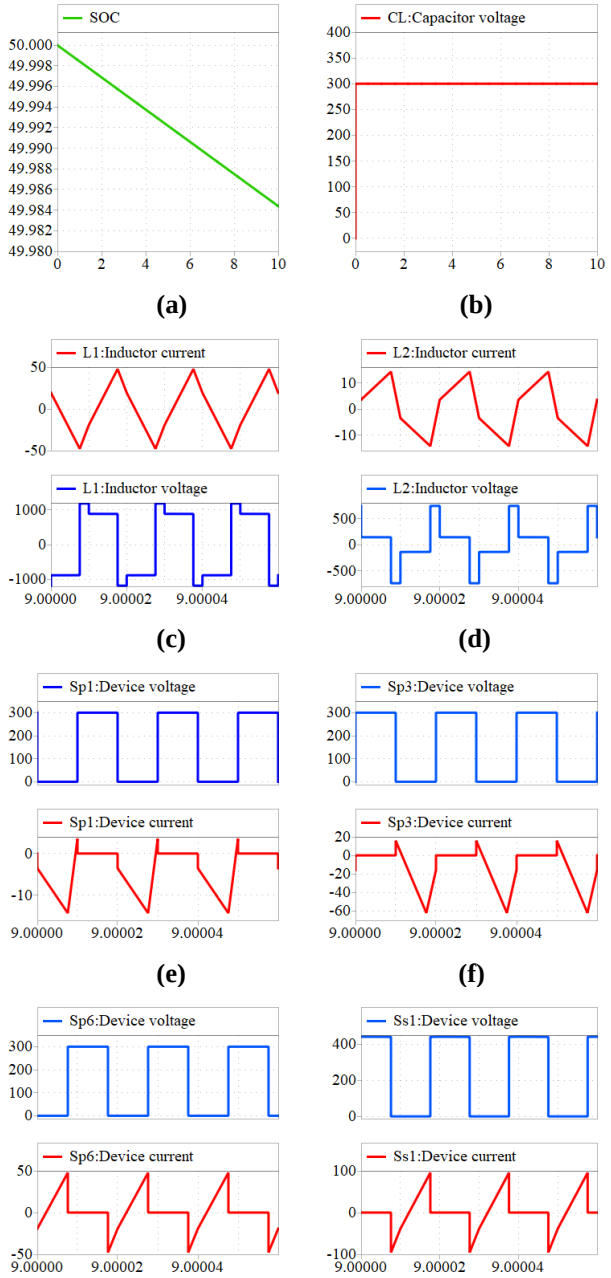

Fig. 14 The simulated outputs of the converter under normal operation in discharging mode with φ = -0.12; **(a)** state of charge battery; **(b)** input voltage; current and voltage of inductor **(c)** L_1; **(d)** L_2; voltage and current stress of power MOSFET **(e)** S_{p1}; **(f)** S_{p3}; **(g)** S_{p6}; **(h)** S_{s1}.

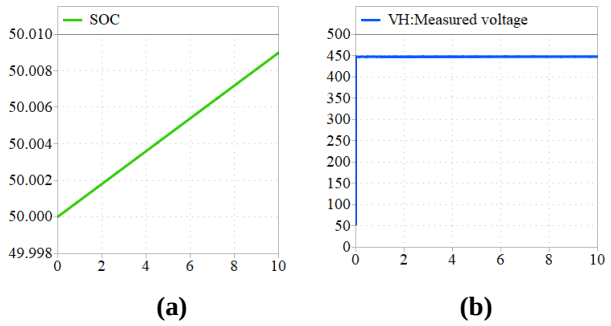

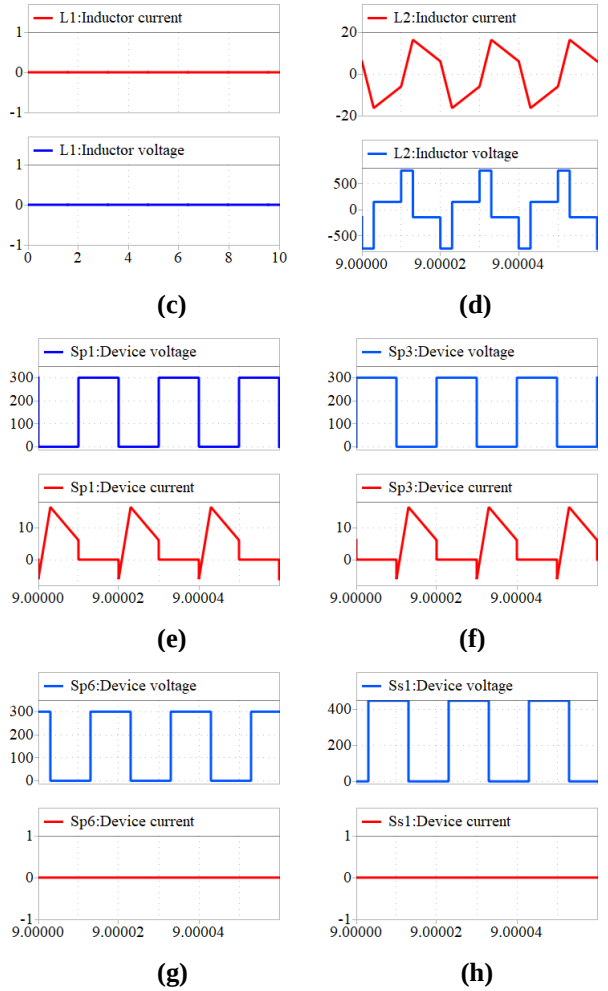

Fig. 15 The simulated outputs of the converter under open-circuit fault of transformer T_{r1} operation in charging mode with φ = 0.15; **(a)** state of charge battery; **(b)** battery voltage; current and voltage of inductor **(c)** L_1; **(d)** L_2; voltage and current stress of power MOSFET **(e)** S_{p1}; **(f)** S_{p3}; **(g)** S_{p6}; **(h)** S_{s1}.

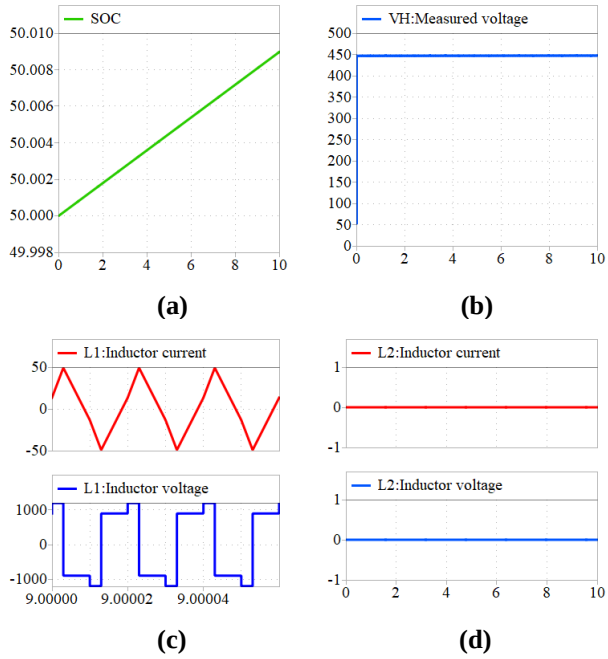

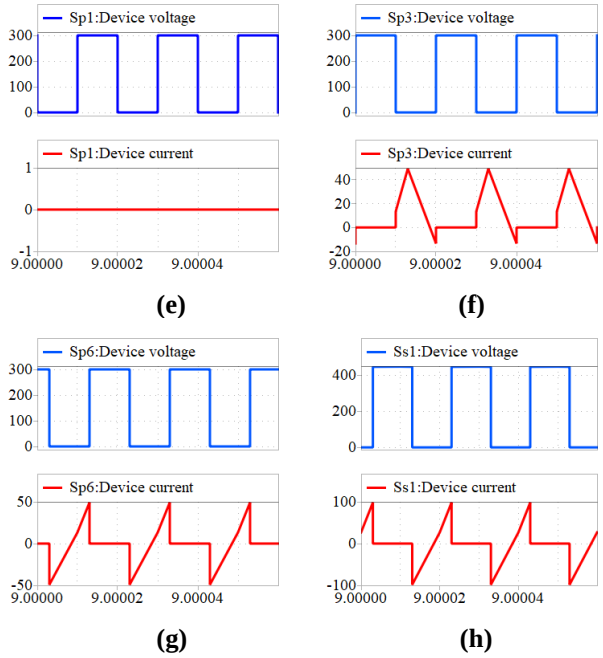

Fig. 16 The simulated outputs of the converter under open-circuit fault of transformer T_{r2} operation in charging mode with $\varphi = 0.15$; **(a)** state of charge battery; **(b)** battery voltage; current and voltage of inductor **(c)** L_1; **(d)** L_2; voltage and current stress of power MOSFET **(e)** S_{p1}; **(f)** S_{p3}; **(g)** S_{p6}; **(h)** S_{s1}.

7 Conclusion

In this paper, a new dual-transformer-based DAB converter has been presented. The characteristics that are intrinsic to a DAB converter, such as the utilization of power MOSFETs in ZVS conditions and the ability of bidirectional power transmission, are present in this converter. Moreover, the proposed converter has the ability to operate even under the open-circuit failure of one of the transformers. Although the power of the converter is halved, the reliability of DAB is increased. Eventually, the accurate battery model was simulated to validate the performance of the proposed converter in electric vehicle applications for charging and discharging the battery. All simulation results confirm that the proposed topology can be the nominated candidate for the bidirectional DC-DC converter used in BEVs.

Acknowledgment

Under grant No. 4005030, the Iran National Science Foundation (INSF) provided research grants for the completion of this project.

References

[1] M. Babalou, M. Dezhbord, M. Maalandish, S. H. Hosseini, M. R. Islam, and H. Torkaman, "Modular DC-DC converter with reduced current ripple and low voltage stress suitable for high voltage applications," *International Journal of Circuit Theory and Applications*, vol. 50, no. 11, pp. 4027-4044, Jul. 2022.

[2] M. Babalou, M. Dezhbord, R. S. Alishah, and S. H. Hosseini, "A soft-switched ultra high gain dc-dc converter with reduced stress voltage on semiconductors," in *10th International Power Electronics, Drive Systems and Technologies Conference (PEDSTC)*, 2019: IEEE, pp. 677-682.

[3] M. Dezhbord, M. Babalou, P. Mohseni, M. R. Islam, L. E. Vafaei, and S. H. Hosseini, "An extendable soft-switched high step-up converter with near zero-ripple input current suitable for fuel cell-powered applications," *IET Renewable Power Generation*, vol. 16, no. 15, pp. 3287-3298, Aug. 2022.

[4] A. Rahali, K. El Khadiri, and A. Tahiri, "Li-Ion Battery Charger Interface Circuit with Fast and Safe Charging for Portable Electronic Devices," *Iranian Journal of Electrical and Electronic Engineering*, vol. 19, no. 1, pp. 2527-2527, 2023.

[5] A. Gallaj, F. Ardashir, and M. Beiraghi, "High Step-Up Interleaved DC/DC Converter Using VM Cell for PV Applications," *Iranian Journal of Electrical and Electronic Engineering*, vol. 18, no. 4, pp. 2503-2503, 2022.

[6] P. Biswal, V. V. S. K. BHAJANA, and P. Drabek, "Investigation of Novel Transformerless Converters for DC Microgrid: Design and Analysis," *Iranian Journal of Electrical and Electronic Engineering*, vol. 18, no. 4, pp. 2557-2557, 2022.

[7] H. Torkaman and T. Hemmati, "Hybrid Z-Source DC-DC Converter with ZVZCS and Power Transformer Resetting: Design, Modeling, and Fabrication," *Iranian Journal of Electrical & Electronic Engineering*, vol. 14, no. 1, p. 49, 2018.

[8] F. Barmoudeh and A. Salemnia, "A Novel Continuous Input Current High Step up DC-DC Converter for Low Level DC Voltage Resource Applications," in *14th Power Electronics, Drive Systems, and Technologies Conference (PEDSTC)*, 2023: IEEE, pp. 1-5.

[9] S. Mohamadian and H. Azizi Moghaddam, "Conduction and Dead-Time Voltage Drops Estimation of Asymmetric Cascaded H-Bridge Converters Utilizing Level-Shifted PWM Scheme," *Iranian Journal of Electrical and Electronic Engineering*, vol. 16, no. 1, p. 48, 2020.

[10] S. Khosrogorji, M. Ahmadian, H. Torkaman, and S. Soori, "Multi-input DC/DC converters in connection with distributed generation units–A review," *Renewable and Sustainable Energy Reviews*, vol. 66, pp. 360-379, Dec. 2016.

[11] H. Torkaman, E. Afjei, A. Keyhani, and M. Poursmaeil, "Control and management of hybrid AC/DC microgrid based on Γ-Z-source converter," *IET Generation, Transmission & Distribution*, vol. 14, no. 14, pp. 2847-2856, Jun. 2020.

[12] H. Torkaman, S. Khosrogorji, and A. Keyhani, "Multi-input converters for distributed energy resources in microgrids," *Microgrids for Rural Areas: Research and Case Studies*, pp. 279-330, 2020.

[13] H. Torkaman, M. Fakhari, H. Karimi, and B. Taheri, "New frequency modulation strategy with she for h-bridge multilevel inverters," in *4th International Conference on Electrical Energy Systems (ICEES)*, 2018: IEEE, pp. 157-161.

[14] H. Khaligh, H. Torkaman, and A. Ebrahimian, "Novel algorithm for optimum output passive filter design in 400 Hz inverter," in *9th Annual Power Electronics, Drives Systems and Technologies Conference (PEDSTC)*, 2018: IEEE, pp. 335-340.

[15] S. K. Rastogi, S. S. Shah, B. N. Singh, and S. Bhattacharya, "Mode Analysis, Transformer Saturation, and Fault Diagnosis Technique for an Open-Circuit Fault in a Three-phase DAB Converter," *IEEE Transactions on Power Electronics*, vol. 38, no. 6, pp. 7644-7660, Jun. 2023.

[16] C. Liu, S. Liu, Y. Chen, X. Zou, and Y. Kang, "Hybrid-type DAB Converter with DC Blocking Capacitor for Ultra-Wide Input-Voltage Range," *IEEE Transactions on Power Electronics*, Jun. 2023.

[17] S. Shao, H. Chen, X. Wu, J. Zhang, and K. Sheng, "Circulating current and ZVS-on of a dual active bridge DC-DC converter: A review," *IEEE Access*, vol. 7, pp. 50561-50572, 2019.
[18] F. Z. Peng, H. Li, G.-J. Su, and J. S. Lawler, "A new ZVS bidirectional DC-DC converter for fuel cell and battery application," *IEEE Transactions on power electronics*, vol. 19, no. 1, pp. 54-65, Jan. 2004.
[19] K. Kim and H. Cha, "Split-capacitor dual-active-bridge converter," *IEEE Transactions on Industrial Electronics*, vol. 68, no. 2, pp. 1445-1453, Feb. 2021.
[20] G. Li, D. Yang, B. Zhou, Y.-F. Liu, and H. Zhang, "Integration of Three-Phase LLC Resonant Converter and Full-Bridge Converter for Hybrid Modulated Multioutput Topology," *IEEE Journal of Emerging and Selected Topics in Power Electronics*, vol. 10, no. 5, pp. 5844-5856, Oct. 2022.
[21] D. Chen, J. Deng, B. Zhang, Z. Wang, and S. Wang, "A dual-transformer based hybrid semidual active bridge converter for wide voltage range applications utilizing simple segmented control," *IEEE Transactions on Power Electronics*, vol. 37, no. 2, pp. 1435-1446, Feb. 2022.
[22] D. Sha, J. Zhang, and K. Liu, "Leakage inductor current peak optimization for dual-transformer current-fed dual active bridge DC–DC converter with wide input and output voltage range," *IEEE Transactions on Power Electronics*, vol. 35, no. 6, pp. 6012-6024, Jun. 2020.
[23] G. Xu, D. Sha, Y. Xu, and X. Liao, "Dual-transformer-based DAB converter with wide ZVS range for wide voltage conversion gain application," *IEEE Transactions on Industrial Electronics*, vol. 65, no. 4, pp. 3306-3316, Apr. 2018.
[24] D. Chen, J. Deng, W. Wang, and Z. Wang, "A Dual-Transformer-Based Hybrid Dual Active Bridge Converter for Plug-in Electric Vehicle Charging to Cope With Wide Load Voltages," *IEEE Transactions on Industrial Electronics*, vol. 70, no. 2, pp. 1444-1454, Feb. 2023.
[25] Y. Liang, X. Liu, G. Xu, and S. Yue, "A dual-transformer-based bidirectional DC–DC converter of using blocking capacitor for wide ZVS range," *IEEE Access*, vol. 8, pp. 170568-170578, Sept. 2020.
[26] M. Babalou, H. Torkaman, E. Pouresmaeil, and M. Dezhbord, "Dual-Transformer-Based DAB Converter With Asymmetrical Power Transmission and High-Power Density for Electric Vehicles," *IEEE Journal of Emerging and Selected Topics in Power Electronics*, vol. 12, no. 2, pp. 1742-1753, Jan. 2024.
[27] M. Chen and G. A. Rincon-Mora, "Accurate electrical battery model capable of predicting runtime and IV performance," *IEEE transactions on energy conversion*, vol. 21, no. 2, pp. 504-511, 2006.